DETERMINATION OF FRACTURE TOUGHNESS
AND FRACTURE ENERGY OF BRITTLE MATERIALS
UNDER IMPACT WEDGING

A. S. Eremenko, S. A. Novikov. V. A. Sinitsyn,
V. A. Pushkov, and M. M. Yakupov

UDC 539.375

1. Test Procedure. Modern fracture mechanics is characterized by an advanced mathematical apparatus and a high level of experimental facilities [1]. The available theoretical and experimental methods allow one to determine criterion parameters for various types of loading. Standard methods of determination of fracture toughness K_{1c} in statics, K_{1d} in dynamics, and the dynamic stress intensity factor (SIF) in crack growth K_D or arrest K_{1a} have been developed [2, 3].

In high-speed loading for a characteristic loading time of $(1–5) \cdot 10^{-3}$ sec and smaller using standard loading schemes, difficulties arise which are due to dynamic effects.

We used stress-wave loading of a specimen by the Hopkinson split bar (HSB) method to determine the fracture toughness and fracture energy of brittle materials under high-speed loading.

Hopkinson proposed to determine stresses in a shock-wave pulse propagating in a bar under explosive loading from the rebound velocity of a measuring bar which is butt-joined with a loading bar [4]. The fracture stresses of brittle materials under tension are considerably lower than those under compression, and a spall forms in bars under intense pulse loading. Khanukaev [5] determined critical spalling stresses in rocks (granite, marble, etc.) from the velocity of the part spalled from the bar, using the Hopkinson method.

Ivanov [6] reported determination of fracture energy in spalling experiments using the integral energy criterion. Kol'skii improved the Hopkinson method. He proposed to measure the wave velocities of transmitted pulses and to compute stresses and strains in a specimen placed between two bars using measured parameters of incident, reflected, and transmitted pulses [7]. Later, the HSB method led to many applications in various types of uniaxial dynamic loading experiments, including determination of fracture toughness.

Novikov [8] reported experiments on determination of the dynamic fracture toughness of hard alloys loaded by the HSB method. Specimens in the form of disks (tablets) with a through central cut loaded in the diametric direction were tested.

An original procedure for determining the fracture toughness of steels and alloys was proposed by Kostin et al. [9]. A bar having a ringed cut with a sharp (fatigue) crack in the base of the cut is subjected to shock-wave loading. As a specimen, the part of the bar neighboring the cut is studied. According to the HSB method, the stresses and forces P in the section of the crack and also the strains δ due to its opening are determined and a quasi-static $P - \delta$ diagram is constructed and analyzed by the standard method. The dynamic fracture toughness K_{1d} and the fracture energy G_c are determined from the $P - \delta$ diagram. In the case of plastic materials, the calculation is performed using the J-integral.

The growth rate of SIF is

$$\dot{K}_1 = K_{1d}/\tau_*,\tag{1.1}$$

where τ_* is the characteristic time of increase in load from zero to a load that corresponds to a critical state. The attainable loading rate for steels is of the order of 10^6 (MPa $\cdot$ m$^{1/2}$) sec^{-1}. This is approximately two orders of magnitude higher than that obtained using the standard loading scheme. The minimum duration of

quasi-static loading is limited by the duration of a transient wave process τ^0 which is due to the appearance of a shear wave and a surface Rayleigh wave on a inhomogeneity (a cut or a crack). In a first approximation the duration is

$$\tau^0 = D/c_2 \tag{1.2}$$

(D is the bar diameter and c_2 is the shear-wave velocity). The actual duration of the high-frequency transient is greater, but it is quickly attenuated owing to considerable material damping in the crack zone.

Kostin et al. [9] showed experimentally that τ^0 could be used as an estimate of the limiting (minimum) duration of quasi-static loading. The limitation of the method is the quite obvious restriction on the type of investigated materials. A procedure for determining K_D based on computational and experimental analysis of crack propagation in a plate in tension with a lateral cut is described in [10].

Procedures for determining the dynamic fracture toughness using the HSB method and a compact wedging specimen are proposed in [11, 12]. The standard eccentric-tension specimen (CT-specimen in the international terminology) modified for loading by wedging is used as the base one. To this end, a wedge-shaped slot is made in specimen 1 and a wedge-shaped striker 2 is fixed rigidly to the loading bar 3 (Fig. 1). The force diagrams of the quasi-static loading of the specimen are calculated by the Kol'skii scheme. The displacement of the wedge as a solid in penetrating into the specimen takes the form

$$U_A(t) = c_0 \int_0^\tau [\varepsilon^+(t) - \varepsilon^-(t)] \, dt,$$

and the displacement of the bearing surface of the second bar 4 is

$$U_B(t) = c_0 \int_0^\tau \varepsilon(t) \, dt.$$

Here c_0 is the elastic-wave velocity in the bars; ε^+, ε^-, and ε are, respectively, the incident, reflected, and transmitted strain pulses registered by strain gages 5 and 6. According to the laws of wave mechanics, we have $\varepsilon^+(t) + \varepsilon^-(t) = \varepsilon(t)$.

It must be taken into account that the sign of ε^- is opposite to that of ε^+, i.e., this expression gives the difference between the absolute values of $\varepsilon^+(t)$ and $\varepsilon^-(t)$. The strain of the specimen δ in the force direction takes the form

$$\delta = U_A - U_B.$$

In quasi-static loading of the specimen, the wedging force can be calculated from the formula

$$P(t) = ES\varepsilon(t) \tag{1.3}$$

(E and S are the modulus of elasticity and cross-sectional area of the bar), and the strain is determined by the approximate formula

$$\delta(t) = -2c_0 \int_0^\tau \varepsilon^+(t) - \varepsilon(t) \, dt, \tag{1.4}$$

where the initial transient phase which lasts only for a few microseconds is ignored, since strains in this phase are very small. The $P - \delta$ diagram is derived by elimination of time from relations (1.3) and (1.4).

The critical force P_*, which corresponds to the onset of fracture and is used to calculate K_{1d}, is determined from the $P - \delta$ diagram by standard analysis. The SIF growth rate is determined by (1.1).

Different methods can be used to calculate K_{1d} from the critical force P_*. One of these uses conversion of the axial wedging force P to the transverse force F related to P by
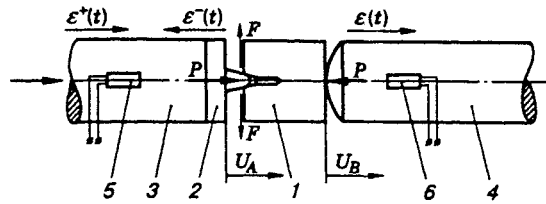
$$F = \frac{P}{2\tan\left(\alpha + \tan^{-1}\varphi\right)}$$
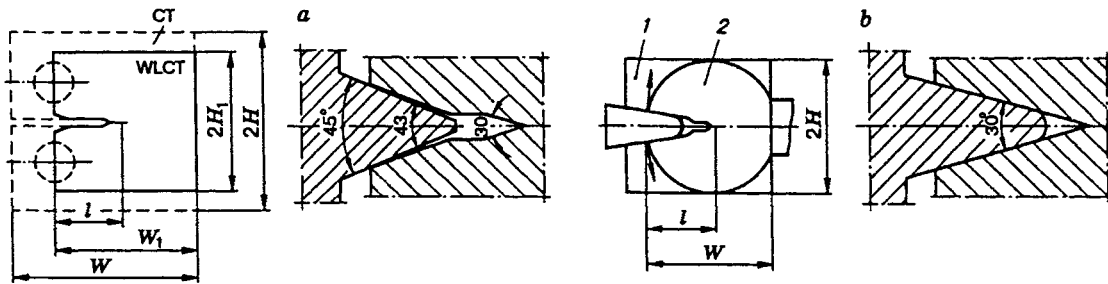
Fig. 1

Fig. 2

(α is the semi-angle of the wedge and φ is the coefficient of friction between the wedge and the specimen), and then K_{1d} is calculated using the standard formula

$$K_{1d} = \frac{F_* l^{1/2}}{BW} f\left(\frac{l}{W}\right), \qquad \dot{K}_1 = \text{const.} \tag{1.5}$$

Here B and W are the thickness and width of the specimen; l is the length of the initial crack; and $f(l/W)$ is the tarring function of compliance (K-tarring). Such an approach is used in [12, 13], where a WLCT wedging specimen (wedge loaded compact tension specimen) shown in Fig. 2a is proposed. In [12] the K-tarring function of the WLCT specimen is computed by the finite-element method. In the region of working lengths of cracks ($0.45 < l/W < 0.55$), the K-tarring function is close to that of the standard CT specimen (curves CT and WLCT in Fig. 3).

Analysis of the given loading scheme has demonstrated that the result is significantly affected by the friction coefficient. It has been proposed [13] to measure the friction coefficient φ directly on the WLCT specimen. The thus measured value of φ for a steel specimen is equal to 0.14 and is used in calculations. The influence of friction has also been investigated by Efimov et al. [14–16] in comprehensive studies of loading by wedging schemes. In the given loading scheme, the specimen and the wedge are in contact in a narrow zone, which prevents a considerable decrease in the friction forces between the specimen and the wedge. The actual friction coefficients for various materials are 0.18–0.3 [15].

The alternative method proposed in this paper involves calculation of K_{1d} from the wedging force P_* using (1.5) and experimental K-tarring of the sample. The difference between the loading scheme used by the authors, in which the standard specimen was also taken as a base (Fig. 2b), and the above-mentioned schemes is that transfer of loading is carried out over the entire lateral surface of the wedge. This is because this method is intended for sufficiently brittle and low-strength nonmetal materials.

The contact surfaces of the specimen and the wedge are treated by a special lubricant to eliminate the influence of friction. Because of the low contact pressures (several megapascals) and small displacements δ (0.03–0.6 mm) in tests of brittle materials, favorable conditions for lubricating are produced and the coefficient of friction is considerably decreased. Under these conditions, the coefficient of friction by our estimate is not greater than 0.05. Another advantage of such a loading scheme is the high rigidity of loading.

Experimental K-tarring is performed by the method of compliance using the well-known Irwin–Kise
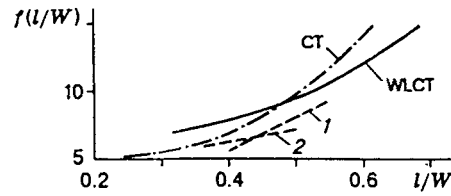
Fig. 3

relation [17]:

$$K_1^2 = \frac{P^2 E^0}{2B} \frac{1}{1 - \mu^2} \frac{d\chi}{dl}.$$

Here $\chi = \delta/P$ is the compliance of the specimen determined by the $P - \delta$ diagram for various lengths of cracks; E^0 and μ are the modulus of elasticity and Poisson's ratio for the specimen material. The obtained tarring functions $f_1(l/W)$ and $f_2(l/W)$ for specimens of rectangular and disk-like configurations (types 1 and 2 in Fig. 2b) are presented in Fig. 3 (curves 1 and 2, respectively). They were approximated in the operating range of lengths of cracks by the linear relations

$$f_1 = -5.4 + 27l/W \quad \text{for} \quad 0.43 < l/W < 0.55,$$

$$f_2 = -0.2 + 14l/W \quad \text{for} \quad 0.4 < l/W < 0.55.$$

The results of SIF determination using K-tarring data were compared with those obtained on standard materials (polymethyl methacrylate and epoxy) by the photoelastic method; the difference does not exceed 10%.

The transient time in specimens is conveniently estimated by relations (1.2) where, in the given case, D is a typical dimension (diameter or height) of the specimen [$D = 2H$ (Fig. 2b)]. For the adopted dimensions ($D = 20$–30 mm), the duration is 25–30 μsec.

The high-speed loading process is conveniently estimated by the relative loading rate ν defined as the reciprocal of τ_*:

$$\nu = \frac{\dot{K}_1}{K_{1d}} = \frac{K_{1d}}{\tau_*} \frac{1}{K_{1d}} = \frac{1}{\tau_*}.$$

The limiting loading velocity under quasi-static loading conditions is $\nu_* = (3\text{–}4) \cdot 10^4$ sec^{-1}. In this case, the dynamic effects due to the longitudinal and transverse inertia of the specimen do not exceed 6% of P_*, as estimated by the formulas given in [13].

It should be noted that in tests using the given loading scheme, the rigid regime is performed as in tests of a double-cantilevered beam specimen (DCB). In this case, as is known, two regimes of crack propagation can be observed: controlled fracture, in which the crack-propagation velocity is determined by the compliance of the specimen and by increase in the loading rate, and unsteady accelerated crack propagation. These regimes are realized in materials with a strong dependence of the fracture energy γ on the crack-propagation velocity V, for example, in polymers. The velocity dependence $\gamma(V)$ was determined in the controlled-fracture regime. To this end, the crack propagation velocity was measured experimentally. At crack velocities not higher than 200–300 m/sec, the fracture energy is given by the quasi-static relation

$$G_c = \gamma = \frac{1 - \mu^2}{E^0} K_{1d}^2, \tag{1.6}$$

in which the kinetic energy of the sample is ignored.

2. Experimental Technique. The experiments were performed on an experimental setup including a loading mechanism, an explosive device, a recorder, and equipment for high-speed photographic recording. Loading was carried out using an explosive device similar to that described previously [18]. The small mass
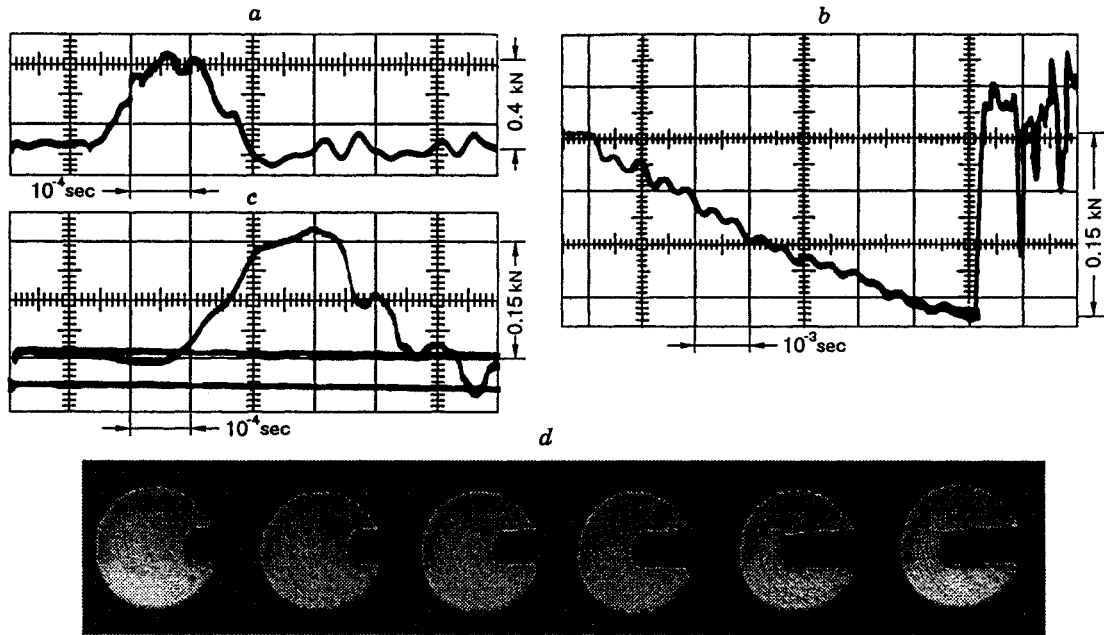
Fig. 4

of the explosive charge (0.1–0.5 g) and safe electric blasting cap ensure safe operations under laboratory conditions.

High-speed photography was performed by an VFU photo recorder. Brittle current-conducting failure gages were used to measure crack-propagation velocity in opaque materials; their signals were transmitted to an SBP-5 oscillograph through a signal-generating unit. The crack velocity was determined by $l - t$ diagrams of crack growth which were constructed using framing camera records and oscillograms. Measurements of dynamic strains were carried out by a standard certified procedure with a measurement error not greater than 12%. At present measurements and data processing are carried out using a computer complex. With a small modification of the setup, tests can be performed at lower loading rates typical of standard methods. In this case, loading is performed by a freely falling striker.

3. Results of the Experiments. The standard methods of determining fracture toughness proceed from the presence of an initial crack in a specimen. In brittle materials, cracks are generally produced by calibrated impacts on a wedging striker inserted into a cut or a slot with a sharpened base. For a number of reasons, controlled growth of an initial crack in some materials, e,g., in granite is hampered. This material has a coarse-grained structure. During crack growth, destruction of granite occurs along glassy intergranular layers. In this case it is difficult to control the length and profile of the initial crack. Similar problems arise with other materials, such as mixed explosives and solid rocket propellants, in which crack propagation is now extensively studied [19].

Methodical problems of testing such materials were solved practically using granite as an example. For testing, granite specimens of the Vyborg deposit were used. They have a rectangular configuration in plane (type 1, Fig. 2b) and dimensions $(2H \times W \times B)$ $20 \times 24 \times 14$ mm and $14 \times 17 \times 8$ mm. Specimens with smaller dimensions were produced from larger broken specimens after their testing. We first studied the structure, the elastic constants E^0 and μ, and also the material density ρ:

$$E^0 = 7 \cdot 10^4 \text{ MPa}, \quad \mu = 0.25, \quad \rho = 2.65 \cdot 10^3 \text{ kg/m}^3.$$

The average grain size measured on the fracture surface is about 1–1.5 mm. The stress intensity of order $1/r^{1/2}$ is known to take place in the vicinity of a cut with finite sharpening radius r at a certain distance greater than r from the tip of the cut. In preliminary static experiments, we determined the maximum sharpening

TABLE 1

Specimen dimensions $B \times W \times 2H$, mm			
8 × 17 × 14		14 × 24 × 20	
K_{1d}, MPa·m$^{1/2}$	ν, 10^4 sec^{-1}	K_{1d}, MPa·m$^{1/2}$	ν, 10^4 sec^{-1}
1.16	0.10	1.18	0.12
1.08	0.11	1.15	0.10
1.20	0.8	1.05	1.3
1.10	0.95	1.16	1.4
1.15	1.2	1.18	1.5
1.20	2.5	1.28	2.6
1.19	3.1	1.10	1.8

radius r_* of a wedge-like cut or a slot for which fracture was governed by an inner defect (in granite it is an intergranular layer of thickness d_*).

The tests showed that for $0.1 < r < 0.7$ mm the fracture stresses in a specimen with a wedge-like cut or a slot does not depend on r. With allowance for the grain size the result can be written as the empirical relation $r_* \leqslant 0.5d_*$, which held in our experiments. In tests of some other materials with a coarse-grained structure a similar result was obtained. Some types of ceramics, graphite, beryllium alloys, mixed explosives, and solid rocket propellants belong among these materials. All experiments were performed at normal temperature. For granite, we obtained $K_{1c} = (1.1 \pm 0.1)$ MPa·m$^{1/2}$.

Dynamic experiments with high-speed loading were performed for loading rates of $10^3 < \nu < 3 \times 10^4$ sec^{-1}. The $P(t)$ oscillograms in Fig. 4a and $P - \delta$ diagrams (Fig. 5, diagram 1) demonstrate the brittle character of fracture. The maximum point P_*, as can be seen from Fig. 5, was used as the critical force P_1.

The values of K_{1d} for granite are listed in Table 1. In the studied range of loading rates, K_{1d} does not depend on the loading rate and is $\langle K_{1d} \rangle = 1.16$ MPa·m$^{1/2}$. A series of similar experiments was performed under low-speed shock loading at loading rate $\nu = (0.5-1) \cdot 10^2$ sec^{-1}. In these experiments a value of $K_{1d} = 1.12$ MPa·m$^{1/2}$ was obtained.

The formula $K_{1d} = \sigma_* \sqrt{\pi l_*}$ can be used to estimate the fracture toughness for granite at maximum strain rates ($\varepsilon \sim 10^6$ sec^{-1}) attained in spalling experiments. Khanukaev [5] obtained spalling strength $\sigma_* = 17$–19 MPa using the Hopkinson method. Assuming that $l_* = 1.2$ mm (grain size), we find the average value of the dynamic fracture toughness: $\langle K_{1d} \rangle = 1.1$ MPa·m$^{1/2}$. Thus, the results indicate that the fracture toughness of granite does not depend on crack velocity over the practically realized range of loading rates. Because of the absence of rate dependence of fracture toughness, systematic measurements of crack velocity were not performed. The average crack velocity was measured to be $V = 90$–100 m/sec (at $\nu \sim 10^4$ sec^{-1}) in several experiments. The fracture energy of granite determined by (1.6) was $G_c = \gamma = (18 \pm 0.5)$ J/m^2.

The behavior of polymers differs greatly from that of granites by the sensitivity to various loading rates. We performed experiments with specimens of transparent organic glasses based on polymethyl methacrylate (PMMC) and polycarbonate (PC), which are linear non-cross-linked polymers. These materials are known to undergo elastic-brittle transition, which manifests itself by embrittlement of these materials at high loading rates or low test temperatures. The temperature–rate relation of the deformation properties of these materials is due to shear high-elasticity (SHE).

The deformability properties are most pronounced for the characteristic loading time τ_* close to the relaxation time τ^+ of the main relaxation process (α-transition). For PC and PMMC at normal temperature, the values of τ^+ vary from 10^{-1} to 10^0 sec, which corresponds to a loading rate of $\nu_* \cong 5$ sec^{-1}.

With an increase in the loading rate ($\nu > \nu_*$) the HSB process "is frozen" and material is embrittled. Numerous experiments performed by the standard procedure [20] using DCB specimens showed that the
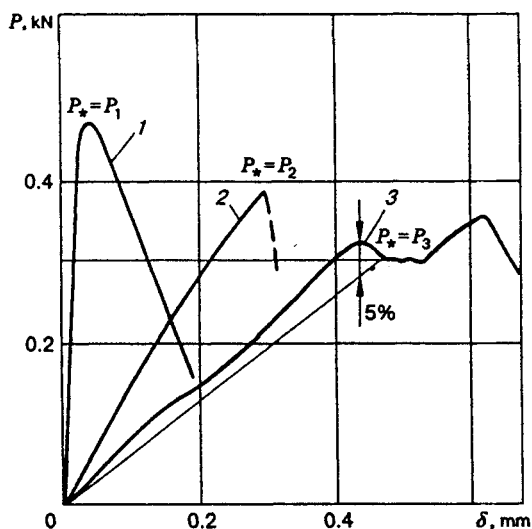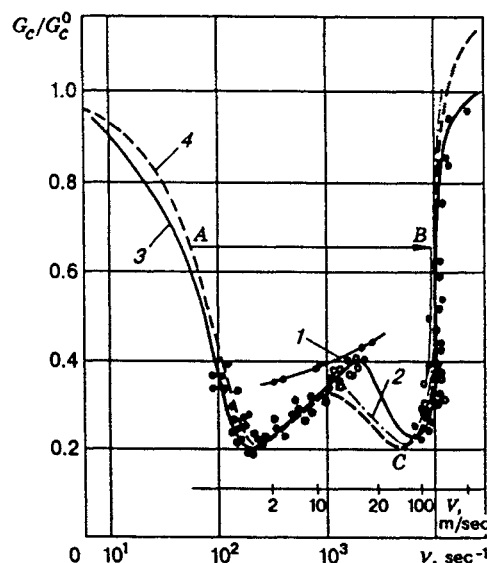
Fig. 5

Fig. 6

dependences of the fracture toughness K_{1c} and fracture energy γ of these materials on the loading rate and the crack growth velocity have a maximum which correlated with the maximum of the relaxation characteristics in similar relations. For PMMC, these data seem to be obtained for the first time in [21]. Analysis of the data of [21, 22] gives the following maximum values of fracture toughness (in statics): $K_{1c} = 2.0$ MPa·m$^{1/2}$ for PMMC and $K_{1c} = 3.5$ MPa·m$^{1/2}$ for PC at loading rates of 1–10 sec^{-1} and crack velocities of $(1-7)\cdot 10^{-2}$ m/sec. At higher loading rates the fracture toughnesses of PC and PMMC are sharply decreased.

At the same time, at high crack velocities ($V > 200$ m/sec), the fracture toughnesses of these materials is considerably increased: $K_D = 2.5$ MPa · m$^{1/2}$ for PMMC and $K_D = 3.45$ MPa · m$^{1/2}$ for PC at $V = 200$–400 m/sec [23], as determined by optical methods (photoelastic and shadow methods [3]). The region of intermediate velocities is less investigated and the results of different authors contradict to one another in some cases.

Thus, the dependence $\gamma(V)$ obtained for PMMC by the DCB [17] method differs from the data in [10] obtained for static tension of sheet specimens (curves 1 and 2 in Fig. 6). Our experiments were conducted at normal temperature at loading rates of $10^3 < \nu < 2 \cdot 10^4$ sec^{-1} using the HSB method, and at lower loading rates ($10^2 < \nu < 10^3$ sec^{-1}) the specimen was affected by a falling load; disk-like specimens with diameters of 20 and 30 mm were used. The specimen thickness was varied from 6 to 12 mm, and an initial crack was present in the specimens. Systematic measurements of crack-growth velocity in the specimens were preformed. Photographic records of crack propagation for time interval between frames $\Delta\tau = 13$ μsec is shown in Fig. 4d.

Typical $P(t)$ oscillograms and $P - \delta$ diagrams at various loading rates are shown in Figs. 4 and 5. They illustrate the existence of two regimes of crack propagation. In low-speed loading, the crack velocity increases sharply after initiation (Fig. 4b) and the $P-\delta$ diagram is of a brittle character (Fig. 5, diagram 2). In high-speed loading, the diagrams indicate steady crack growth after initiation with an increase in load (Figs. 4c and 5). Determination of K_{1d} from the such diagrams was performed by the standard 5% secant method (Fig. 5, diagram 3). The values of K_{1d} and γ were estimated from the obtained diagrams and expressions (1.5) and (1.6). The experiment results show that in the early stage of growth (in the regime of steady growth) the crack velocity V and the value of SIF are roughly constant due to the rigid loading scheme and the flat function of compliance (Fig. 3). This allows one to plot the curves of the dynamic SIF K_D and the fracture energy γ versus the crack-growth velocity.

The obtained results are shown in Fig. 6 as curves of the fracture energy of PC and PMMC (curves 3 and 4, respectively) versus the loading rate and crack-growth velocity in the relative form: as the ratio G_c/G_c^0,
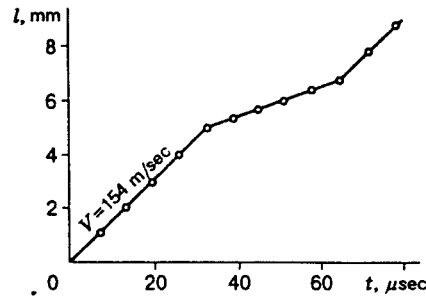
592

Fig. 7

where G_c^0 is the maximum fracture energy for each material under static loading (1.0 kJ/m^2 for PMMV and 3 kJ/m^2 for PC). Experimental points are given only for PC (the dark circles refer to specimens Ø 30 mm and the light circles to specimens Ø 20 mm). The dependence $\gamma(V)$ takes place only in the regime of controlled fracture for $d\gamma/dV > 0$; in this case, the dependences $\gamma(\nu)$ and $\gamma(V)$ are similar (they differ only in the scale on the velocity axis). The results agree with the data of [10, 23], but only qualitatively agree with the data of [17]. The appreciable increase in γ at $V > 100$ m/sec and K_{1d} at $\nu > 10^4$ sec^{-1} is caused by the local heating of the material at the crack tip due to transition to adiabatic conditions and "unfreezing" of the SHV relaxation process. This has been shown experimentally by Fuller et al. [24].

In conclusion, we dwell on the features of the high-speed crack-growth regime observed in the given materials. At a low crack-growth velocity that does not exceed the critical velocity V_* at the beginning of tough-brittle transition, the crack is propagating steadily. If the crack velocity exceeds V_*, it increases sharply and acquires a value that corresponds to the high-velocity branch of the dependence $\gamma(V)$. On the descending branch of the energy dependence $\gamma(V)$ for $d\gamma/dV < 0$ 0, as is shown in [25], the crack cannot propagate in a steady regime. Furthermore, if the supply of elastic energy is limited, the crack-growth velocity, after a certain region of steady growth, decreases rapidly to a value that corresponds to the minimum fracture energy (it is shown in Fig 6 by A–B–C transition). In this regime the crack is growing until the elastic energy of the body is exhausted. Under dynamic loading this process is additionally affected by elastic waves. The crack velocity can be changed repeatedly under quasistatic loading. A typical $l - t$ diagram of crack growth in the specimen is shown in Fig. 7.

The obtained results indicate the high resolution of quasi-static tests of a compact specimen by the HSB method for revealing subtle features of high-speed fracture. This method is widely used in the Scientific Research Institute of Experimental Physics for dynamic tests of materials used in nuclear power engineering.

REFERENCES

1. V. Z. Parton and V. G. Boriskovskii, *Dynamic Fracture Mechanics* [in Russian], Mashinostroenie, Moscow (1985).
2. V. V. Panasyuk, *Quasi-Brittle Fracture Mechanics* [in Russian], Naukova Dumka, Kiev (1991).
3. V. Z. Parton and V. G. Borisovskii, *Brittle Fracture Dynamics* [in Russian], Mashinostroenie, Moscow (1988).
4. B. A. Hopkinson, "Method of measuring the pressure produced in the detonation of high explosives or by the impact of bullets," *Proc. Roy. Soc.*, **A74**, 498–507.
5. A. N. Khanukaev, *The Energy of Stress Waves in Rock Blasting* [in Russian], Gosgortekhizdat, Moscow (1962).
6. A. G. Ivanov, "Spalling in a quasi-acoustic approximation," *Fiz. Goreniya Vzryva*, **4**, No. 3, 475–480 (1975).

7. H. Kolsky, "An investigation of mechanical properties of materials at very high loading rates," *Proc. Phys. Soc.*, **62**, 676–687 (1949).

8. N. V. Novikov, "On the influence of loading rate on the fracture toughness of hard alloys," *Probl. Prochn.*, No. 10, 61–64 (1980).

9. L. S. Kostin, J. Duffy, and L. B. Freund, "Fracture initiation in metals under stress wave loading conditions," in: *Fracture Mechanics: News in Foreign Science* [Russian translation], No. 25, Mir, Moscow, 151–171 (1981).

10. J. Congleton and B. K. Denton, "Measurement of fast crack growth in metals and nonmetals," *ibid.*, 172–198 (1981)

11. A. P. Bolshakov, A. S. Eremenko, V. L. Lupsha, et al., "Temperature and rate dependences of fracture toughness of polymethyl methacrylate at high rates of loading," *Fiz.-Khim. Mekh. Mater.*, No. 1, 79–82 (1981).

12. A. Andrzejewski, J. Klepaczko, and G. Pluvinage, "Determination experimentale de la tenacite a grande vitesse de chargement d'alliages d'aluminium," *J. Mech. Appl.*, **5**, No. 3, 345–336 (1981).

13. J. Klepaczko, "Discussion of a new experimental method for determining the onset of crack propagation at high loading rates by means of stress waves," in: *Theoretical Principles of Design* (перевести!), **104**, No. 1, 33–40 (1982).

14. V. P. Efimov and E. N. Sher, "Calculation of parameters of rigid-wedge penetration into a specimen with a cut," *Fiz. Tekh. Probl. Razrab. Polezn. Iskop.*, No. 1, 109–113 (1989).

15. V. P. Evimov, "Dynamic calibration of measurements of the fracture toughness of brittle materials by the wedging method," *Fiz. Tekh. Probl. Razrab. Polezn. Iskop.*, No. 4, 89–93 (1990).

16. V. P. Efimov, P. A. Martynyuk, and E. N. Sher, "Allowance for the influence of vertical forces in wedging," *Fiz. Tekh. Probl. Razr. Polezn. Iskop.*, No. 3, 32–36 (1992).

17. K. B. Bucknell, *The Shock-Resistant Plastics* [Russian translation], Khimiya, Leningrad (1981).

18. A. S. Eremenko, S. A. Novikov, and A. P. Pogorelov, "The investigation of propagation and interaction of fast cracks in organic glass," *Prikl. Mekh. Tekh. Fiz.*, No. 4, 109–112 (1979).

19. C. W. Smith, "Experiments in three-dimensional fracture problems," *Exp. Mech.*, **33**, No. 4, 249–258 (1993).

20. V. A. Lupsha and S. A. Novikov, "Effect of temperature and strain rate on the fracture toughness of PMMC," *Fiz.-Khim. Mekh. Mater.*, No. 6, 116–118 (1979).

21. P. I. Vincent and K. V. Gothan, "Effect of crack propagation velocity on the fracture surface energy of polymethyl methacrylate," *Nature*, **210**, 72 (1966).

22. A. A. Kaminskii, *Fracture Mechanics of Viscoelastic Solids* [in Russian], Naukova Dumka, Kiev (1980).

23. M. Ramulu, A. S. Kobayachi, B. S. J. Kang, and D. B. Borher, "Further studies on dynamic crack branching," *Exp. Mech.*, **23**, No. 4, 431–437 (1983).

24. K. N. Fuller, P. G. Fox, and I. E. Field, "The temperature rise at the tip of fast moving cracks in glassy polymers," *Proc. Roy. Soc. London*, **A341**, 537–557 (1975).

25. G. I. Barenblatt and R. L. Salganik, "On wedging of brittle solids. Autooscillations in wedging," *Prikl. Mat. Mekh.*, **27**, No. 3, 436–449 (1993).